Proceedings of the Institute of Acoustics

ON THE VIOLIN FAMILY STRING/BODY DYNAMICAL COUPLING

O Inácio — Instituto Politécnico do Porto, Escola Superior de Música e Artes do Espectáculo Musical Acoustics Laboratory, Rua da Alegria, 503, 4000-045 Porto, Portugal
J Antunes — Instituto Tecnológico e Nuclear, Applied Dynamics Laboratory ITN/ADL, Estrada Nacional 10, 2686-953 Sacavém Codex, Portugal
M C M Wrigth — Institute of Sound and Vibration Research, University Road, Highfield, Southampton S017 1BJ, UK

1 INTRODUCTION

Raman's seminal paper[1] was a landmark pioneer effort on the dynamics of bowed strings. Since then, a plethora of research papers has been published on bowed-string instruments, including enlightening work by Friedlander[2], Schelleng[3], McIntyre, Schumacher and Woodhouse[4], to name just a few classics among many other significant papers (see Cremer's book[5], for an extensive account of the field).

In previous work we developed a modal method to deal with plucked and bowed strings[6-9], enabling an effective simulation of such systems, even when dispersive effects are significant. As in most other published work, our simulations assume a string pinned at the bridge and the nut, and therefore decoupled from the instrument body. Such approach proved adequate to obtain the typical motion patterns displayed by bowed-strings. However, because the bridge is assumed motionless, computations are obviously unable to cope with more subtle phenomena related to the coupling of string and body motions.

A crude approach to incorporate body effects, when simulating string sounds, is to start by computing the vibratory response of an "isolated" (bowed or plucked) string, and then use the resulting string/bridge interaction force to drive a given body vibro-acoustic transfer function. However, this simple approach is quite limited and cannot account for any energy feedback from the body into the string – such as found for instance in "wolf notes" – because no true string/body coupling has been modelled.

To our best knowledge, only a few authors have attempted to address the string/body coupling problem. Schumacher, McIntyre and Woodhouse[4] incorporated in their wave-propagation computational algorithm a bridge-reflexion function which encapsulates the dynamical behaviour of a given body resonance, enabling them to simulate the coupled dynamics between the string and the chosen body resonance. In the same vein, Puaud et al.[10] used in their work (connected with a so-called "numerical bow") a mass-stiffness bridge-resonator, therefore also emulating a chosen body-resonance coupled to the string dynamics. Recently, a different approach has been pursued by several authors to simulate instrument bodies and cavities – see Huang et al.[11], for instance – by using 2D or 3D waveguides to compute simplified multi-degree-of-freedom resonating systems. However, until now, this modelling technique has only been used to simulate the body-filtering effects on string/bridge dynamical forces, with no feedback coupling. In relation to other stringed instruments, Derveaux et al.[12] achieved fully coupled string/soundboard computations for a modelled guitar.

In short, as far as we know, simulation of the interaction between strings and real-life instrument bodies has not yet been attempted. Such is the aim of the present work, where our computational method is extended to incorporate the multi-modal dynamics of a violin and cello body, fully coupled to the string motions. Ours is a hybrid approach, in the sense that a theoretical model of the string is coupled with dynamical body data, stemming from either simplified models or real-life experiments.

The string is modelled using its unconstrained modes and, in contrast with our previous publications[6-9], assuming now pinned-pinned boundary conditions at the tailpiece and the nut. Then, at the bridge location, the string/body coupling is enforced using the body impulse-response or modal data (as measured at the bridge). At each time step, the system motion is computed by integrating the string modal equations, excited by the modal-projected values of the frictional bow force and also of the string/bridge contact force. The latter is obtained from the body motion at each time-step, as computed either (a) using the body impulse-response, or (b) from a modal model of the body. In the first method, the body dynamics are obtained through incremental convolution, a costly procedure which however enables the direct simulation of real bodies without any further modelling assumptions or simplifications. The second method allows for faster computations, but demands a computed or identified modal model of the instrument body. After a few demonstrative experiments and a detailed presentation, our computational approaches are illustrated for both violin and cello typical self-excited string motion regimes. These are compared for "isolated" strings and for the string/body coupled model, based here on synthetic body dynamical data. In particular, interesting simulations pertaining to the so-called "wolf notes" are presented.

2 PRELIMINARY EXPERIMENTS

In order to start exploring the coupling between the body of the instrument and the strings, some preliminary experiments were carried on a cello. Figure 1 shows a typical mobility frequency response function measured at the bridge in the horizontal direction as shown in Figure 2, through impact excitation, the bridge response being sensed by an accelerometer. The main body resonance occurs at approximately 196 Hz with a relatively low damping ratio (z =0.7%) when compared with the majority of the other peaks which reveal damping ratios of the order of 2%. This high amplitude mobility peak (1.6×10^{-1} $ms^{-1}N^{-1}$) is responsible for a particular effect to which these instruments (bad or good) are known to be very susceptible: the wolf note. It is an unpopular phenomenon among musicians since it gives origin to harsh and beating-like sounds turning proper musical execution extremely difficult at some positions along the fingerboard. Although unpleasant for the listener, the emergence of this effect is paradigmatic of the importance of the body/string interaction.

Figures 3 to 5 show several typical bridge velocity responses, and corresponding spectra, to excitation by bowing on the C_2 open string (tuned to 65.4 Hz) at different notes on the fingerboard. Typical velocity amplitudes for the vibration of the bridge at the C_2 open string are shown to be of the order of 0.1~0.2 m/s. At a bowing position of approximately 40 mm from the bridge (Figure 3), the third harmonic is prevailing relatively to the lower order partials. The proximity of its frequency to the frequency of the main body resonance (3 x 65.4 Hz = 196.2 Hz) enhances this particular harmonic revealing the importance of string/body coupling for normal musical regimes.

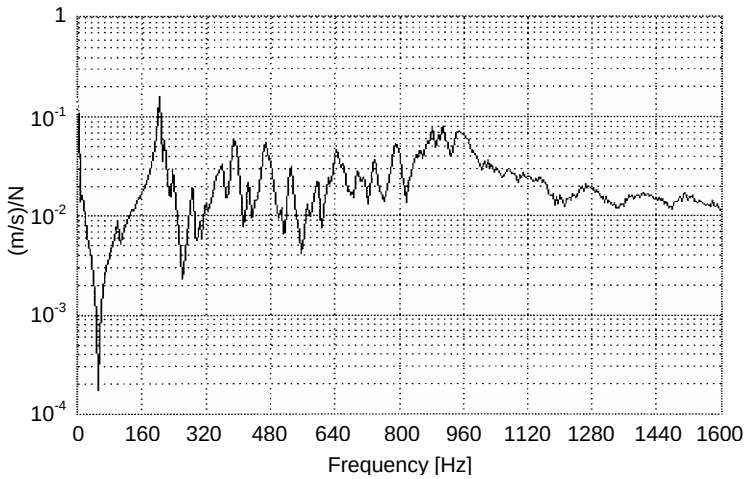

Figure 1 – Mobility transfer function of the cello measured at the bridge.

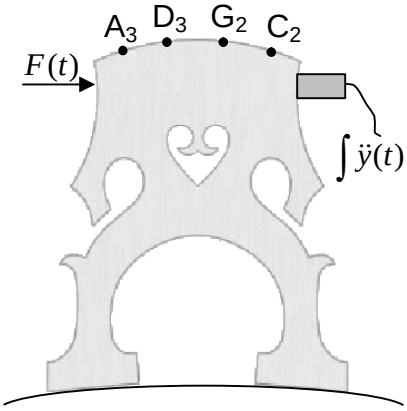

Figure 2 – Setup used for the transfer function measurements.

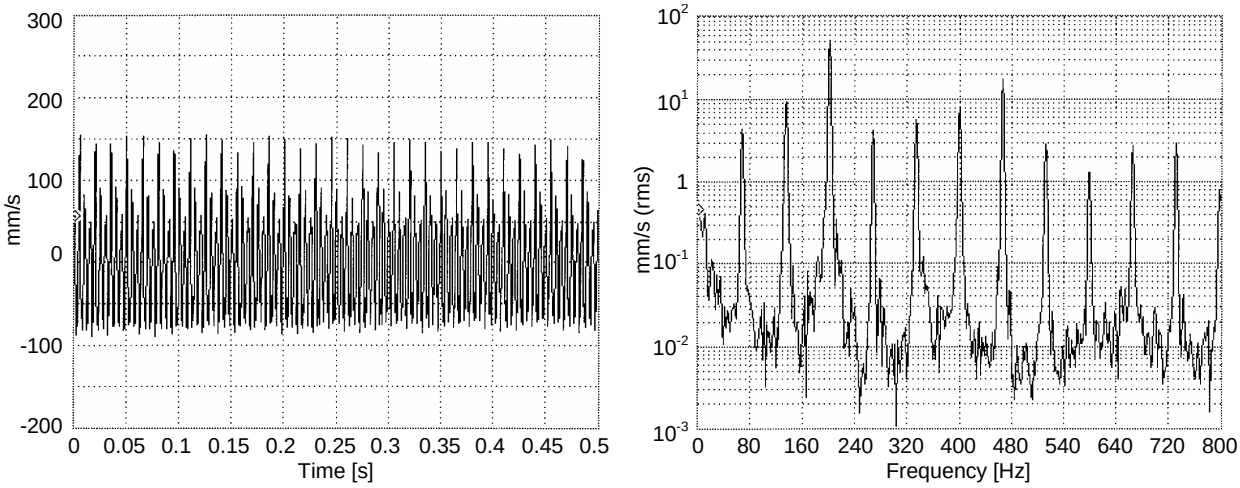

Figure 3 – Velocity time-history and spectrum of the bridge vibration, resulting from bowing on the C_2 open string.

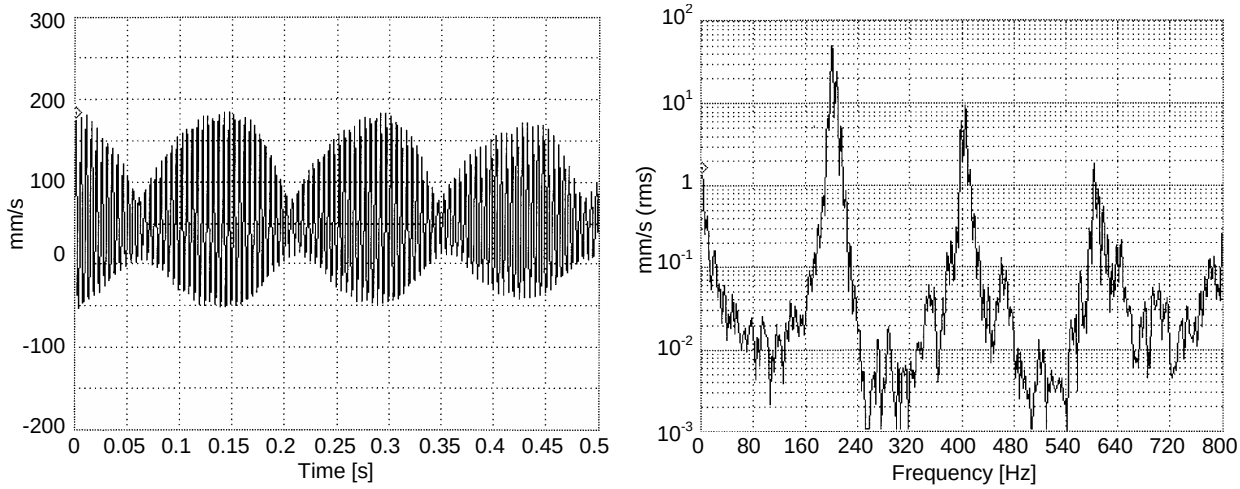

Figure 4 – Velocity time-history and spectrum of the bridge vibration, resulting from bowing on the C_2 string at a fingerboard position approximately $L/3$ from the bridge (generating here a wolf note).

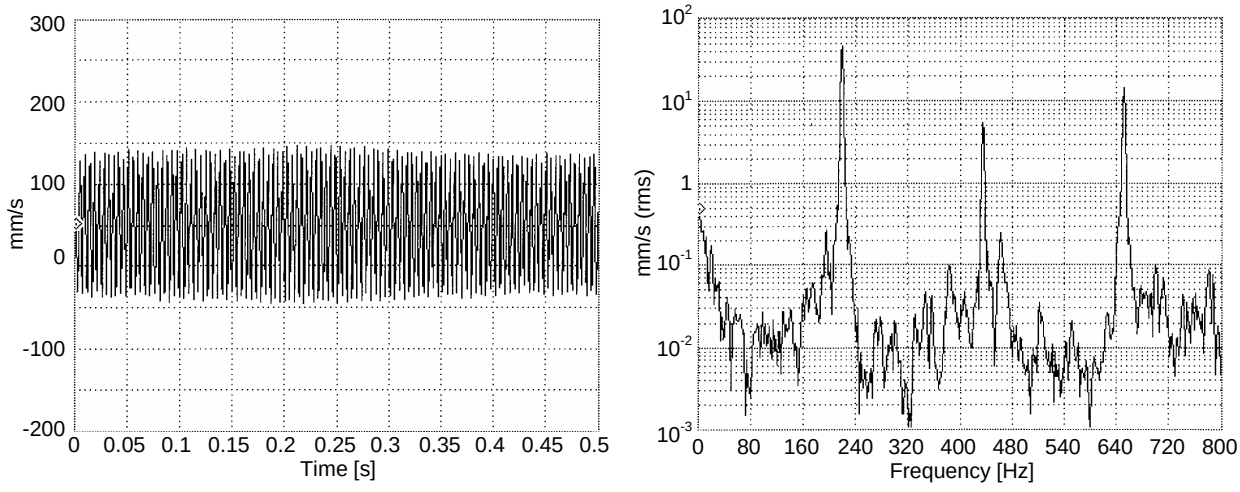

Figure 5 – Velocity time-history and spectrum of the bridge vibration, resulting from bowing on the C_2 string at a fingerboard position about one semitone above the wolf note (compare with Figure 4).

Figure 4 depicts the typical amplitude-modulated waveform that characterizes the wolf note. In order to achieve this sound, the musician stopped the C_2 string at a distance approximately $L/3$ from the bridge (where L is the length of the string), for this instrument, playing the G_3 note at roughly 196 Hz. Clearly, the beating phenomena displayed is the result of strong coupling between the string vibration and the main body resonance, which is related to the proximity of their frequencies. Shortening the effective length of the string by a small amount is enough to prevent the wolf note to develop as can be seen in Figure 5. In this case the finger moved along the fingerboard in the direction of the bridge a few millimetres, which was enough to alter the fundamental frequency of the stopped string to 218 Hz which prevented the strong string/body coupled response.

The wolf phenomenon has been the subject of several papers[1,10,13-18], the most generally accepted explanation being the one suggested by Schelleng[13], forty years ago. More recently the basis of this explanation has been revisited and further discussed by Woodhouse[18]. However, there are still a few aspects deserving exploration, such as the influence of the string dynamics in the portion between the tailpiece and the bridge (see [12] for an interesting experimental account). On the other hand, we experienced a dependence of the wolf beating frequency on the bowing parameters, an aspect which seems absent from the literature. Also, the emergence of wolf phenomena appears to depend somewhat on the time-history of the bowing parameters, a fact which has also been noted in [12]. These issues will be addressed in the present and future papers.

3 COMPUTATIONAL METHOD

3.1 Formulation of the String Dynamics

Consider an ideal string of length L, linear density μ and dissipation coefficient h, subject to a constant axial tensile force T and a force distribution $F(x,t)$. The small-amplitude transverse motion $y_s(x,t)$ of the string is described by the classic damped wave-equation:

$$\mu \frac{\partial^2 y_s}{\partial^2 t} = T \frac{\partial^2 y_s}{\partial x^2} - h \frac{\partial y_s}{\partial t} + F(x,t) \tag{1}$$

where the wave speed is given by $c^2 = T/\mu$. Any solution of equation (1) can be formulated in terms of the string's modal parameters: for modeshapes normalised at unitary maximum values modal masses are given as $m_n = \mu \cdot L/2 \ \ (\forall n)$. Other modal parameters are the circular frequencies $w_n = n\pi c/L$, damping values z_n and mode shapes $j_n(x) = \sin(n\pi x/L)$, with n = 1, 2, …, N. The order N of modal truncation is problem-dependent and must be asserted by physical reasoning. On the modal space the forced response of the damped string is formulated as:

$$[M]\{\ddot{Q}(t)\} + [C]\{\dot{Q}(t)\} + [K]\{Q(t)\} = \{\Xi(t)\} \tag{2}$$

where $[M] = \mathrm{Diag}(m_1,\cdots,m_N)$, $[C] = \mathrm{Diag}(2m_1w_1z_1,\cdots,2m_Nw_Nz_N)$, $[K] = \mathrm{Diag}(m_1w_1^2,\cdots,m_Nw_N^2)$, are the matrices of modal parameters, $\{Q(t)\} = \langle q_1(t),\cdots,q_N(t)\rangle^T$ and $\{\Xi(t)\} = \langle \Im_1(t),\cdots,\Im_N(t)\rangle^T$ are the vectors of modal responses and generalised forces, respectively. The damping values z_n are usually identified from experiments, however, they may eventually be theoretically estimated. The modal forces $\Im_n(t)$ are obtained by projecting the external force field on the modal basis:

$$\Im_n(t) = \int_0^L F(x,t)\ j_n(x)\ dx\ , (n = 1,2,...,N) \tag{3}$$

The physical motions at any point of the string can be computed from the modal amplitudes $q_n(t)$ by superposition:

$$y(x,t) = \sum_{n=1}^{N} j_n(x)\, q_n(t) \tag{4}$$

and similarly concerning the velocities and accelerations. For given external excitation and initial conditions, the previous system of equations can be integrated using an adequate time-step integration algorithm. Explicit integration methods are well suited for the friction model used here. In

our implementation, we used a simple Velocity-Verlet integration algorithm, which is a low-order explicit scheme. Note that, although (2-4) obviously pertain to a linear formulation, nothing prevents us from including in $\Im_n(t)$ all nonlinear effects arising in the system. Accordingly, the system modes become coupled by the nonlinear effects.

For the present case, the external force field $F(x,t)$ is due to the excitation friction force $F_{s,a}(x_c,t)$ provided by the bow (which we will model in this paper as a single hair bow, although we can easily introduce excitation by a bow of finite width – see [9]), by the interaction force $F_b(x_b,t)$ between the body and the string at the bridge and by the possible presence of a finger on the fingerboard (see Figure 6).

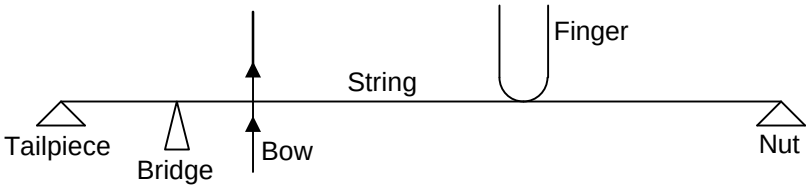

Figure 6 – Idealized model of the bowed string

3.1.1 Friction Model

The friction force arising between the string and the bow hair at location x_c of the string is given by:

$$\begin{cases} F_s(x_c,t) = -m_d(\dot{y}_c)\dfrac{F_N}{b}\,\mathrm{sgn}(\dot{y}_c)\ ;\ \text{if}\ \ |\dot{y}_c| > 0 \\ \qquad |F_a(x_c,t)| < m_S\dfrac{F_N}{b}\ \ ;\ \text{if}\ \ |\dot{y}_c| = 0 \end{cases} \tag{5}$$

where F_N is the normal force between the bow and the string, m_S is a "static" friction coefficient (used during surface adherence) and $m_d(\dot{y}_c)$ is a "dynamic" friction coefficient (used for sliding regimes). Here, the relative transverse velocity between the bow and the string is given by:

$$\dot{y}_c(t) = \dot{y}(x_c,t) - \dot{y}_{bow}(t) = \sum_{n=1}^{N} j_n(x_c)\ \ \dot{q}_n(t) - \dot{y}_{bow}(t) \tag{6}$$

In this work we assume that $m_d(\dot{y}_c)$ is a function of the relative bow/string velocity, and use the following model:

$$m_d(\dot{y}_c) = m_D + (m_S - m_D)\ \ \mathrm{e}^{-C|\dot{y}_c|} \tag{7}$$

where, $0 \le m_D \le m_S$ is an asymptotic lower limit of the friction coefficient when $|\dot{y}_c| \to \infty$, and parameter C controls the decay rate of the friction coefficient with the relative bow/string sliding velocity. The friction model (7) can be readily fitted to typical experimental data, by adjusting the empirical constants m_S, m_D and C.

The sliding behaviour, described by the first equation (5), does not cause problems for simulations, as this equation explicitly shows how the sliding force should be computed as a function of the sliding velocity. However, during adherence, simulation becomes more difficult. Indeed, the second equation (5) merely states a limiting value for the friction force, during adherence, and gives no hint on how $F_a(\dot{y}_c,t)$ may be actually computed. This is because the adherence force depends on the overall balance of all internal and external forces acting upon the system, which are quite complex for multi-degree of freedom problems. Most friction algorithms deal with this problem through implicit numerical schemes, which can be quite expensive to run. In our approach, the following explicit procedure is used at each time-step *i*:

(1) If in the previous time-step the system was sliding, we start by detecting a possible bow-hair/string adherence, by computing $J_i = \dot{y}_c(t_i) \cdot \dot{y}_c(t_{i-1})$. Then, if $J_i > 0$, the system is still sliding in the same direction. We compute $F_s(\dot{y}_c, t_i)$ according to the first equation (5), with $\dot{y}_c(t_i)$ given by equation (6) and $m_d(t_i)$ by equation (7).

(2) However, if $J_i \leq 0$, then a reversal of the relative motion is occurring and adherence will arise. Then, we compute the sticking force using the following model:

$$F_a(x_c, t_i) = -K_f \; y_c(t_i) - C_f \; \dot{y}_c(t_i) \tag{8}$$

which will be used during the complete duration of the adherence state. The idea in equation (8) is to "attach" the string to the bow at point x_c using a suitable "adherence stiffness" and to damp-out any residual bow/string relative motion during sticking using an "adherence damping" term in equation (8). y_c is the relative displacement between the string and the bow hair, at any time during adherence, given as:

$$y_c = y(x_c, t) - y^a_{bow}(t) = \sum_{n=1}^{N} j_n(x_c) q_n(t) - y^a_{bow}(t) \tag{9}$$

where $y^a_{bow}(t)$ is the current position of the bow "attachment point". For a given constant bow speed, this changes as $y^a_{bow}(t) = (t - t_a)\, \dot{y}_{bow}$, where t_a is the time value when adherence was detected. Constants K_f and C_f are established as explained in [9].

(3) After computing the adherence force, $F_c(\dot{y}_c, t_i)$ is compared with the maximum allowable value $m_S F_N$. If $|F_a| \leq m_S F_N$, the current estimate is accepted and simulation continues assuming a sticking state. On the contrary, when $|F_a| > m_S F_N$, sliding will arise and the friction force is recomputed according to the first equation (5). Then, the procedure continues with the next time-step. We stress that, by virtue of (6) and (9), all the string modes become coupled when the nonlinear friction force is projected on the modal basis, equation (3), and then incorporated in equation (2).

3.2 Formulation of the Body Dynamics

As previously explained, our method was implemented to simulate the influence of the string/body coupling using two different procedures: incremental convolution of a measured impulse response or through a modal model of the body dynamics.

3.2.1 Incremental Convolution Formulation

At the bridge, the string motion forces the violin body into vibration. The response of the body can be computed, at each time step i, by the incremental convolution of the time-history of the interaction force between the bridge and the string $F_b(x_b, t)$ and the body impulse response function at the same point x_b , according to equations (10) and (11).

$$y_b(x_b, t) = \int_0^t F_b(x_b, t) \cdot h(t - t)\, dt \quad ; \quad \dot{y}_b(x_b, t) = \int_0^t F_b(x_b, t) \cdot \dot{h}(t - t)\, dt \tag{10,11}$$

where $y_b(x_b, t)$ and $\dot{y}_b(x_b, t)$ are the displacement and velocity of the bridge at the contact point with the string, while $h(t)$ and $h(t)$ are the displacement/force and velocity/force impulse response functions of the instrument body, measured at the bridge.

3.2.2 Modal Formulation

The response of the body of the instrument can be represented by a simplified modal model:

$$[M_B]\{\ddot{Q}_B(t)\} + [C_B]\{\dot{Q}_B(t)\} + [K_B]\{Q_B(t)\} = \{\Xi_B(t)\} \tag{12}$$

where $[M_B] = \text{Diag}(m_1^B, \cdots, m_P^B)$, $[C_B] = \text{Diag}(2 m_1^B w_1^B z_1^B, \cdots, 2 m_P^B w_P^B z_P^B)$, $[K_B] = \text{Diag}\left(m_1^B (w_1^B)^2, \cdots, m_P^B (w_P^B)^2\right)$, are the matrices of the body modal parameters, $\{Q_B(t)\} = \langle q_1^B(t), \cdots, q_P^B(t) \rangle$ and $\{\Xi_B(t)\} = \langle \Im_1^B(t), \cdots, \Im_P^B(t) \rangle^T$ are the vectors of modal responses and generalized forces, respectively. The modal forces $\Im_p^B(t)$ are obtained by projecting the string/body coupling force $F_b(x_b, t)$ (see section 3.3), on the body modal basis. The modal parameters are identified from a single transfer function measurement at the bridge. This fact leads to a requirement that the modal mass matrix should be normalised by postulating all modeshapes $j_p^B(x_b)$ unitary at the bridge location. The physical motions at the bridge are then computed from the modal amplitudes $q_p^B(t)$ and velocities $\dot{q}_p^B(t)$ by superposition:

$$y_b(x_b, t) = \sum_{p=1}^{P} q_p^B(t); \qquad \dot{y}_b(x_b, t) = \sum_{p=1}^{P} \dot{q}_p^B(t) \tag{13,14}$$

3.2.3 Discussion of the Body Dynamics Formulation Methods

Both methods described before have advantages and disadvantages from the computational point of view. The incremental convolution method allows the use of measured impulse response functions of real-life instruments, without any other assumptions other than linearity, neither the use of any modal identification procedure. It allows the most accurate representation of the body dynamics, but has the great disadvantage of requiring very long computation times due to the brute-force convolution formulations (10,11). On the other hand, the modal approach of the body allows for much lower computation times (at least by one order of magnitude), but requires a careful modal identification to be performed. Furthermore, the modal representation is less-than-ideal to cope with the body dynamics at higher-frequency modal densities. Computation times are proportional to the number of modes used in the model. In contrast, the incremental convolution procedure computation time does not depend on the modal order but only on the duration of the impulse response function. Finally, it should be emphasised that although not presented in this paper, vertical motion of the string and bridge can be easily implemented with this computational method.

3.3 Formulation of the String/Body Coupling

The coupling between the string and the body of the violin arises from the bridge/string contact force $F_b(x_b, t)$ which is used in equations (2), (10), (11) and (12). In this paper we model this interaction by connecting the string to the bridge through a very stiff spring with some dissipation to avoid any parasitic oscillations of the coupling oscillator:

$$F_b(x_b, t) = K_{bs} \cdot \left[y_b(x_b, t) - y_s(x_b, t) \right] + C_{bs} \left[\dot{y}_b(x_b, t) - \dot{y}_s(x_b, t) \right] \tag{15}$$

where K_{bs} and C_{bs} are stiffness and damping coupling coefficients between the bridge and the string, and $y_s(x_b, t)$ and $\dot{y}_s(x_b, t)$ are the displacement and velocity of the string at the bridge.

4 SIMULATION RESULTS

Simulations were performed for both a violin and a cello. To test the behavior of our coupled computational method we will focus on the movement of a violin G-string with a fundamental frequency of 196 Hz, an effective length L = 0.33 m and a linear density of $m = 3.1 \times 10^{-3}$ kg/m. In order to achieve adequate computational convergence we have used 60 modes and a sampling frequency of 20000 Hz. A modal damping value of 0.1% was used for all modes (however, frequency dependent damping can be easily introduced with this method) and a string inharmonicity coefficient B was introduced to provide more realistic simulations[3,5]. This effect is easily simulated using our approach, as the bending stiffness influence is automatically incorporated in the string modes, with modified frequencies according to:

$$w_n = n \cdot w_1 \sqrt{1 + B \cdot n^2} \tag{16}$$

where $B = p E f^4 / 64 L^2 T$ for homogeneous strings. However, the lower strings for the violin or cello are usually wound and therefore non-homogeneous, so we explored some available experimental data and use B = 2.3x10^{-4} (inferred from Table 4.9 of reference[19]).

Concerning the friction model, we chose to use a classic sliding law such as the one presented in equation (7), with m_S = 0.4, m_D = 0.2 and C = 5, which produced realistic results. For the adherence model a total value of K_f = 10^5 N/m as been used. As previously discussed, a near-critical value of the adherence damping term C_f was adopted[9,10]. In this context, it should be mentioned that recent research results[20] suggest the relevance of dynamical thermal phenomena in the tribology of rosin, which may induce hysteretic effects in the friction-velocity dependence. In spite of the unquestionable interest of such findings, we will use here the classical approach for sliding behavior, as the present paper addresses a different issue.

The stiffness and damping constants values, K_{bs} and C_{bs}, used for the string/body coupling were chosen in order to enable a very stiff connection, while keeping a satisfactory computational convergence. We used values of K_{bs} = 10^7 N/m and C_{bs} = 100 Ns/m.

4.1 Violin Simulation Results

Figures 7 to 9 show simulations of the violin string and bridge dynamics for different boundary conditions, when applying a normal bow force (F_N) of 1 N and bow velocity ($\dot{y}_{bow}$) of 0.1 m/s. Figure 7 shows the most widely simulated case of a string pinned at the bridge and the nut (with a length of 0.330 m). Perfect reflections arise from these extremities and the Helmholtz motion is clearly perceptible. The force at the bridge is easily computed from the modal time responses $q_n(t)$, through a superposition of the modal reaction forces, equation (17), where f_1 is the fundamental frequency of the string.

$$F_b(t) = -4\rho m L f_1^2 \sum_{n=1}^{N} n\, q_n(t) \tag{17}$$

Figure 8 represents the case of a string pinned at the tailpiece and the nut, with a total length of 0.385 m, a rigid bridge being placed at 0.330 m from the nut. The same overall behaviour as in the previous example could be expected, since there is no movement of the bridge. However, note that the string inharmonicity enables some energy to pass to the tailpiece-side of the string, leading to low-amplitude waves at higher frequency. Superposed to the well known bow-bridge secondary waves shown in Figure 7, these parasitic oscillations are clearly perceptible in the string/bridge coupling force shown in Figure 8. This effect, already noted by Puaud et al.[10], can be seen very clearly on the computed animations of the string motion. Nevertheless, not unexpectedly, a Helmholtz motion similar to the previous example developed. Notice that the overall behaviour of the string-bridge contact force is similar for the computations in Figures 7 and 8. This is a reassuring feature, accounting that in Figure 7 the contact force is computed from the modal summation of equation (17), while in Figure 8 the interaction force stems from the totally different approach stated in equation (15).

Figure 9 shows the results obtained from the simulations computed through the implementation of the string/body coupling by application of the modal model of a violin body (section 3.2.2). A modal identification was performed on an average-quality violin and 13 modes were chosen to represent the essential features of its dynamical behavior. The corresponding synthesized impulse response function was also calculated and used in the incremental convolution method, leading exactly to the same results. As in the previous example, the oscillations of the tailpiece side of the string can also be seen in the string/bridge coupling force.

The similarity of the plots depicted in Figures 8 and 9 is due to the high impedance presented by the violin bridge to the string waves, which are – in this computation – hardly affected by the comparatively negligible bridge motion. However it is important to emphasise that such result was obtained when bowing an open G-string, with a fundamental frequency significantly lower than the first body resonance (at about 276 Hz). However, in contrast to this situation, interaction between the string and the body can be much stronger when playing notes with frequencies close to body resonances. Then, bridge motion amplitude (and energy string/body interplaying) may become very significant, as typically experienced in cellos when playing wolf notes. Typically, the cello string suffers a much greater influence from the body, as was clear from the experiments shown in Figures 3 and 4.

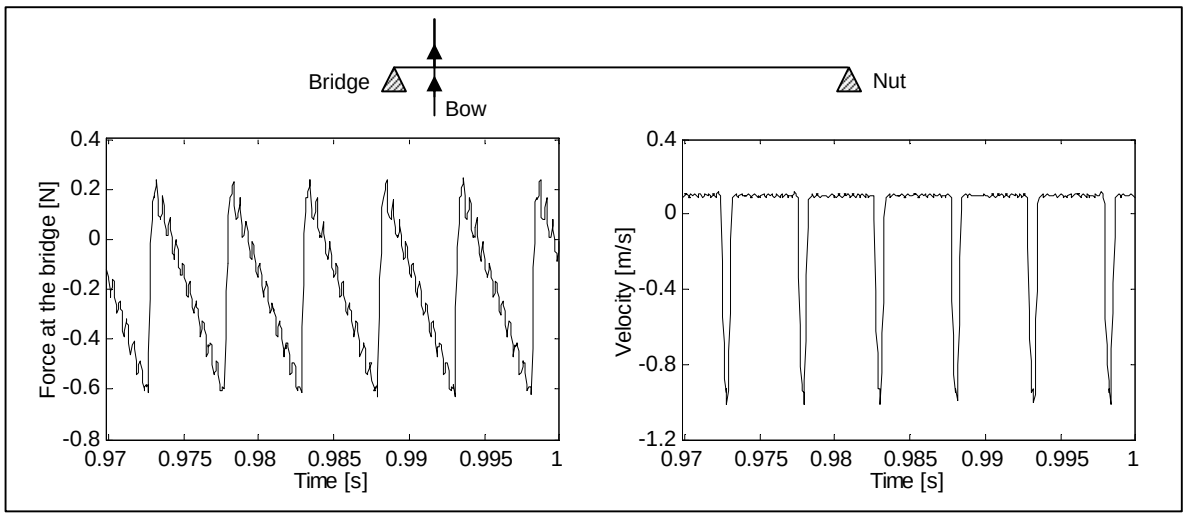

Figure 7 – Force at the bridge and string velocity at the bow contact point for a 0.330 m string pinned at both extremities (F_N = 1 N, $\dot{y}_{bow}$ = 0.1 m/s).

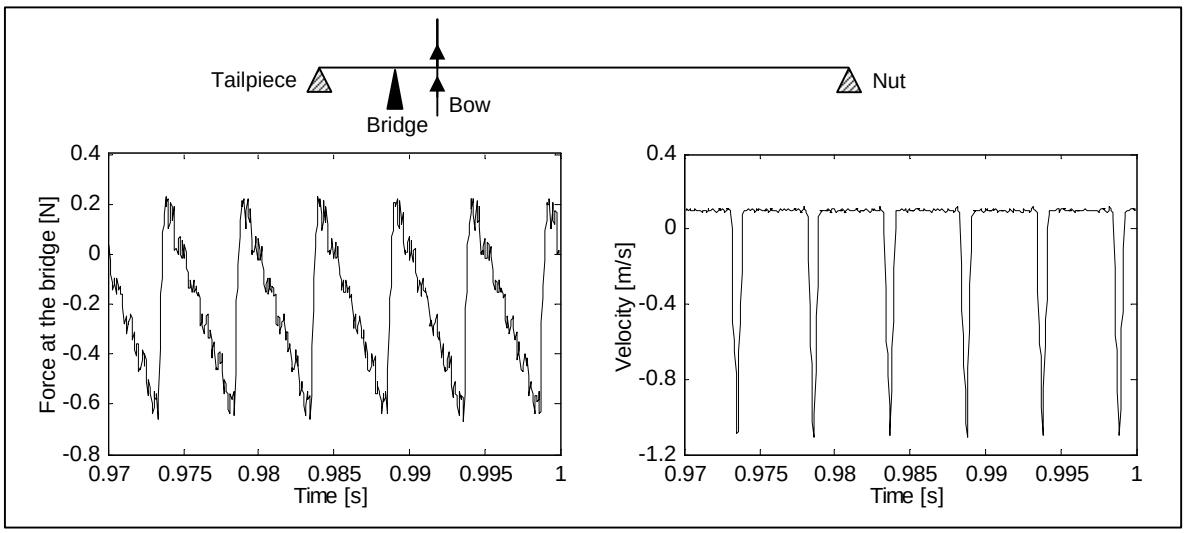

Figure 8 – Force at the bridge and string velocity at the bow contact point for a 0.385 m string pinned at the nut and tailpiece (rigidly supported bridge at 0.330 m, F_N = 1 N, $\dot{y}_{bow}$ = 0.1 m/s).

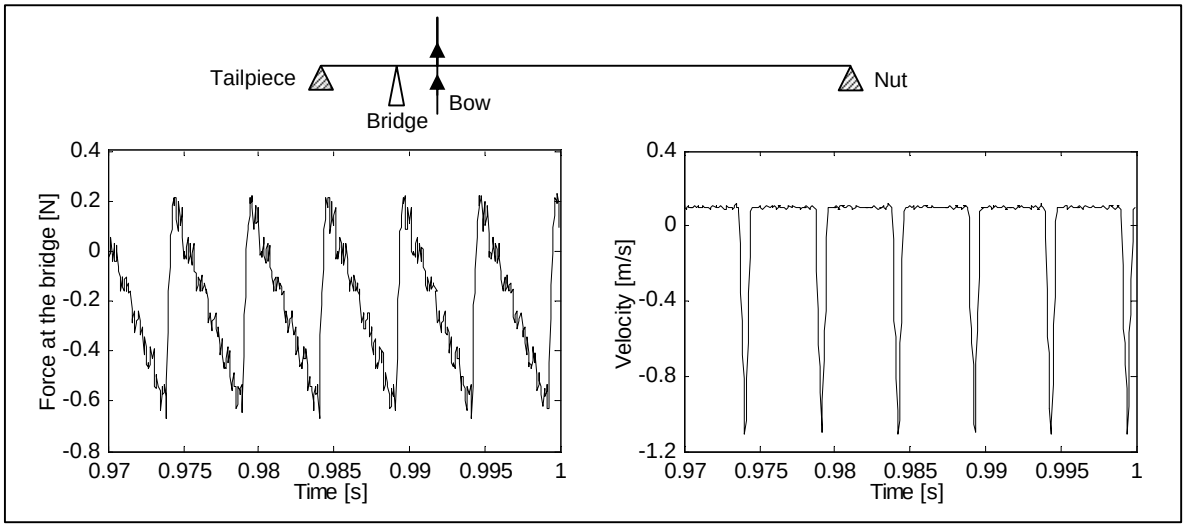

Figure 9 – Force at the bridge and string velocity at the bow contact point for a 0.385 m string pinned at the nut and tailpiece (flexibly supported bridge at 0.330 m, F_N = 1 N, $\dot{y}_{bow}$ = 0.1 m/s).

Simulations of plucked violin strings were also performed for the uncoupled and coupled cases. Figure 10 (a) and (b) depict the velocity of the string at the plucking point for these two conditions. In the uncoupled case (a), the string motion decreases in a simple exponential manner, while in the coupled situation (b) the interaction with the body dynamics can be clearly seen. Furthermore, additional energy is transferred from the string and dissipated at the body of the instrument, originating a higher motion decay rate. Calculation of the logarithmic decrement gave damping factors of the order of 0.2% in the uncoupled case and 0.4% in the coupled case.

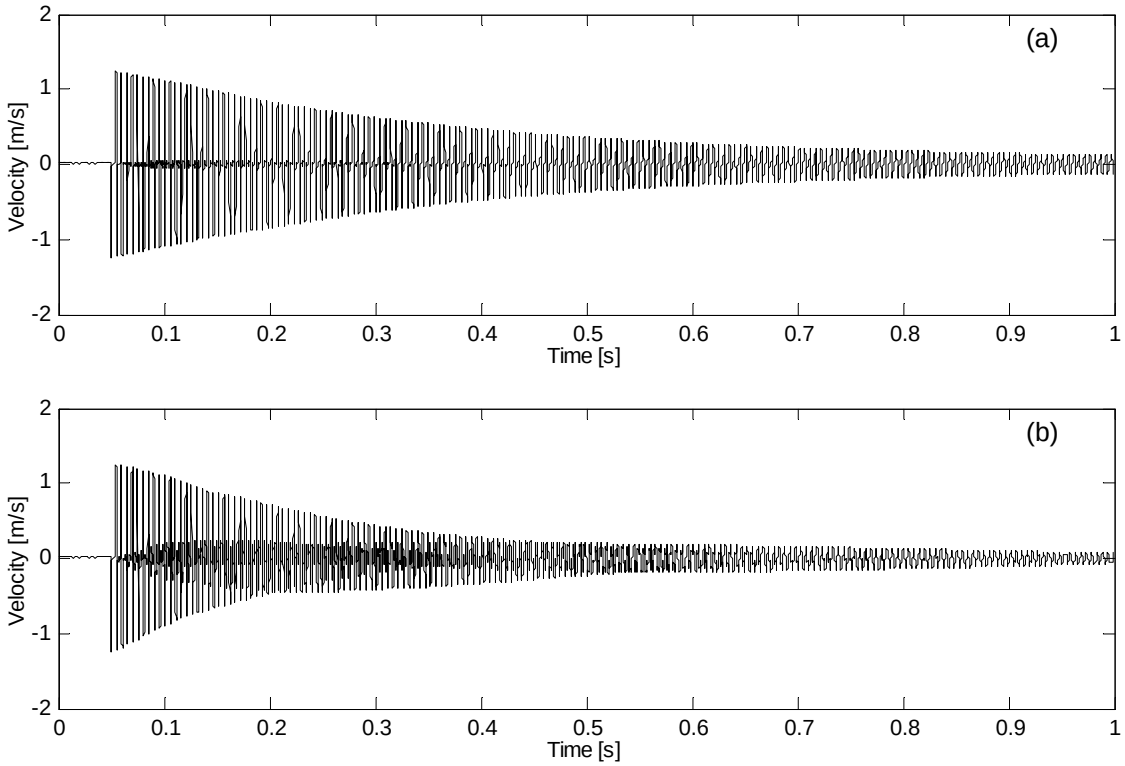

Figure 10 – Simulation of a plucked G-string coupled (a) and uncoupled (b) to the instrument body.

4.2 Cello Simulation Results

As the influence of the cello body on the dynamics of its C_2 string was so apparent during the preliminary experiments, we performed several coupled simulations for this instrument using a modal representation of this instrument body as crudely identified from the frequency response function in Figure 1. To detect easily the emergence of a possible wolf note, a glissando was implemented in the simulation-scheme by moving a finger along the fingerboard in the range x_f = 260~210 mm relatively to the bridge – *upward glissando* – or x_f = 210~260 mm – *downward glissando*. To simulate the force exerted by a moving finger on the string, the "finger" was pragmatically modelled using three spring/dashpots of adequate stiffness/dissipation at coordinates [x_f - 5 mm , x_f , x_f + 5 mm].

The results are presented in Figures 11 to 14, which represent the bridge velocity, for different bowing conditions. The wolf note emerges approximately between positions 240 mm to 235 mm for the upward glissando, however it does not appear at exactly the same range for the downward glissando as can be seen in Figure 12. Another interesting aspect, which challenges the physical explanations given so far, is the fact that the wolf note beating frequency changes for different bowing conditions. Increasing the bowing velocity originates an increase of the beating frequency (Figure 13), while higher bow normal forces tend to reduce this value (Figure 14).

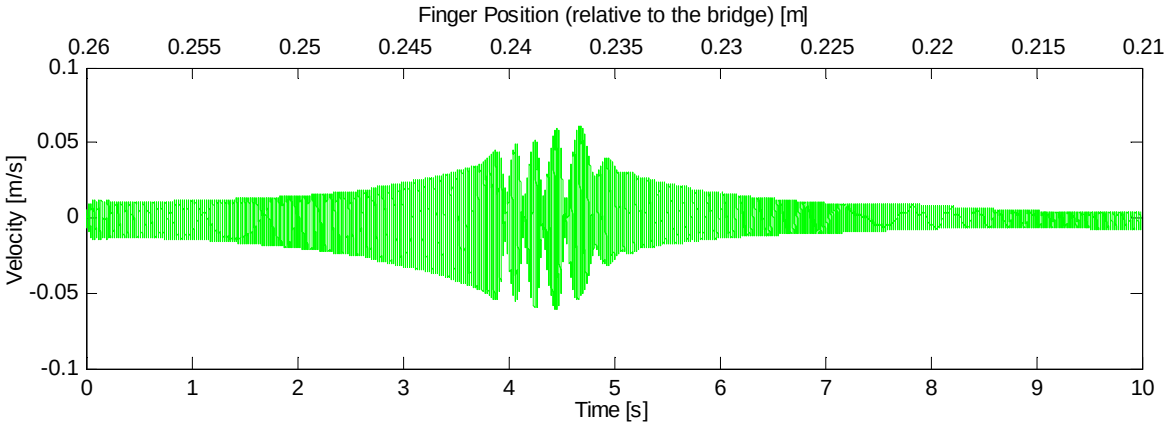

Figure 11 – Simulation of an upward glissando on a cello C-string with F_N = 2 N and $\dot{y}_{bow}$ = 0.1 m/s.

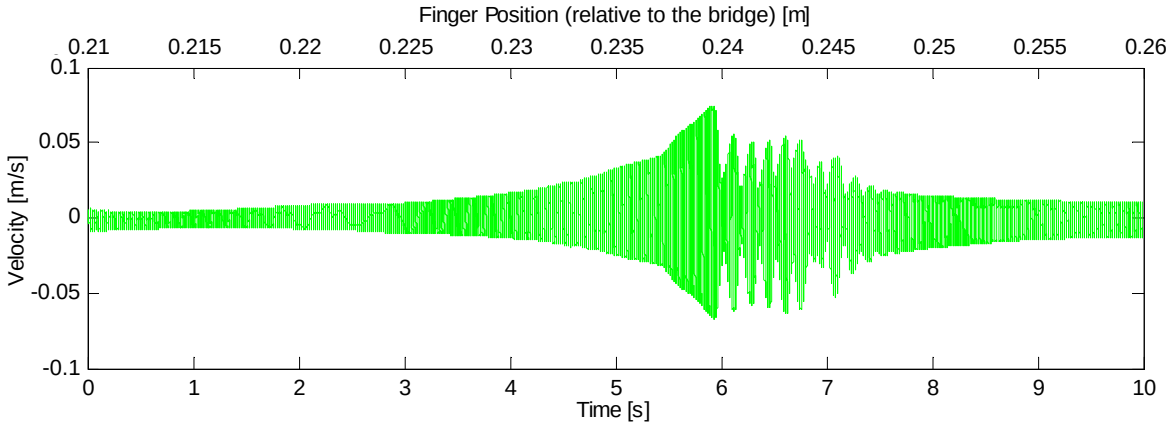

Figure 12 – Simulation of a downward glissando on a cello C-string with F_N = 2 N and $\dot{y}_{bow}$ = 0.1 m/s.

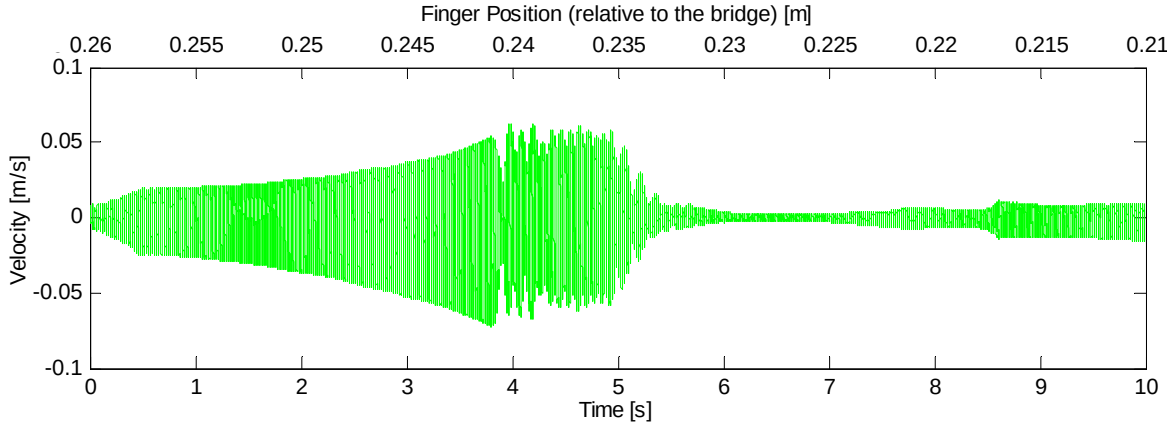

Figure 13 – Simulation of an upward glissando on a cello C-string with F_N = 2 N and $\dot{y}_{bow}$ = 0.2 m/s.

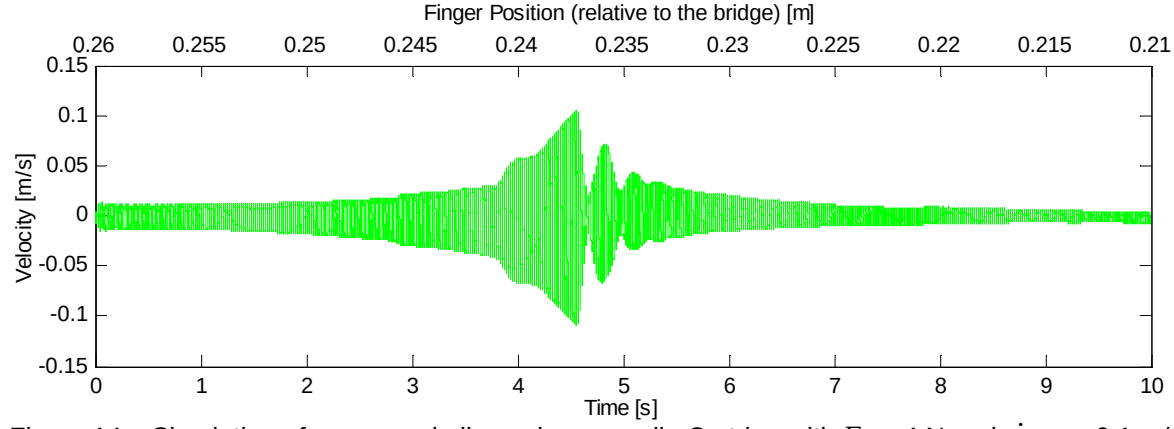

Figure 14 – Simulation of an upward glissando on a cello C-string with F_N = 4 N and $\dot{y}_{bow}$ = 0.1 m/s.

5 CONCLUSIONS

In this paper we propose a significant extension of our bowed/plucked string modelling techniques, in order to incorporate the complex dynamics of real-life instrument bodies, coupled to the string motions. In our hybrid approach, a modelled string interacts with actual or synthesized body data, in the form of bridge impulse response functions or identified modes. Numerical simulations illustrate the Helmholtz motions of an isolated and of a body-coupled violin G-string, for comparative boundary conditions. Computations show that string motions between the bridge and the tailpiece may influence, to some degree, the system dynamics. Our simulations of a cello C-string subjected to glissando playing highlight the string/body interaction, as well as the interesting behaviour of wolf notes, in particular concerning the dependency of the beating frequency on the bowing parameters.

6 REFERENCES

1. C. V. Raman (1918), “On the mechanical theory of the vibrations of bowed strings and of musical instruments of the violin family, with experimental verification of the results”, Indian Association for the Cultivation of Science, Vol 15, pp. 1-158.
2. F. G. Friedlander (1953), “On the oscillations of the bowed string”, Proceedings of the Cambridge Philosophical Society, Vol 49, pp. 516-530.
3. J. C. Schelleng (1973), “The bowed string and the player”, Journal of the Acoustical Society of America, Vol. 53, pp. 26-41.
4. M. E. McIntyre, R. T. Schumacher & J. Woodhouse (1983), “On the oscillations of musical instruments”, Journal of the Acoustical Society of America, Vol. 74, pp. 1325-1345.
5. L. Cremer (1984), “The physics of the violin”, MIT Press, Cambridge, MA.
6. J. Antunes, M. G. Tafasca, L. L. Henrique (2000), “Simulation of the Bowed-String Dynamics: Part 1 – A Nonlinear Modal Approach”, 5e Congrès Français d’Acoustique, Lausanne, Suisse, 3-6 Septembre 2000.
7. M. G. Tafasca, J. Antunes, L. L. Henrique (2000), “Simulation of the Bowed-String Dynamics: Part 2 – Parametric Computations”, 5e Congrès Français d’Acoustique, Lausanne, Suisse, 3-6 Septembre 2000.
8. J. Antunes, L. L. Henrique, O. Inácio (2001), “Aspects of Bowed-String Dynamics”, Proceedings of the 17th International Congress on Acoustics, (ICA 2001), Rome, Italy.
9. O. Inácio, (2002) “Largeur d’Archet et Régimes Dynamiques de la Corde Frottée”, Actes du 6ème Congrès Français d’Acoustique (6ème CFA), Lille, France.
10. J. Puaud, R. Caussé & V. Gibiat (1991), “Quasi-périodicité et bifurcations dans la note de loup”, J. Acoustique, Vol. 4, pp. 253-259.
11. P. Huang, S. Serafin, J. O. Smith (2000), “A Waveguide Mesh Model of High-Frequency Violin Body Resonances”, Proceedings of the International Computer Music Conference (ICMC 2000), pp. 86-89, Berlin, Germany, August 27 - September 1, 2000.
12. G. Derveaux, A. Chaigne, P. Joly, E. Bécache (2003), “Time-domain simulation of a guitar: Model and Method”, Journal of the Acoustical Society of America, Vol. 114, pp. 3368-3383.
13. J. Schelleng (1963), “The Violin as a Circuit”, Journal of the Acoustical Society of America, Vol. 35, pp. 326-338.
14. I. Firth, J. Buchanan (1973), “The wolf in the cello”, Journal of the Acoustical Society of America, Vol. 53, pp. 457-463.
15. A. H. Benade (1975), “The wolf tone on violin family instruments”, Catgut Acoustical Society Newsletter, Vol. 24, pp. 21-23.
16. M. E. McIntyre, J. Woodhouse (1979), “On the fundamentals of bowed-string dynamics”, Acustica, Vol. 43, pp. 93-108.
17. C. E. Gough (1980), “The resonant response of a violin G-string and the excitation of the wolf note”, Acustica, Vol. 44, pp. 113-123.
18. J. Woodhouse (1993), “On the playability of violins: Part 2 – Minimum bow force and transients”, Acustica, Vol. 78, pp. 137-153.
19. E. Jansson (2002), “Acoustics for violin and guitar makers: Chap. 4 – Properties of the violin and guitar string”, (4th Edition), available through http://www.speech.kth.se/music/acviguit4.
20. J. H. Smith, J. Woodhouse (2000), “The tribology of rosin”, Journal of the Mechanics and Physics of Solids, Vol. 48, pp. 1633-1681.